Asian Journal of Chemistry; Vol. 37, No. 12 (2025), 2989-3000
ASIAN JOURNAL OF CHEMISTRY
https://doi.org/10.14233/ajchem.2025.34610

Synthesis of Indole-Thiazolidinedione-1,2,3-triazole Conjugates as Tubulin Polymerization Inhibitors and Some *in silico* Studies

VEERABOINA LINGASWAMY[1], RAJA SHEKHAR KONDRAPOLU[2], ASHOK KUMAR BAPURAM[3], SATHEESH KUMAR NUKALA[4,*] and RAVINDER MANCHAL[1,*]

[1]Department of Chemistry, Chaitanya Deemed to be University, Himayathnagar, Ranga Reddy, Hyderabad-500075, India
[2]Department of Chemistry, University of Arkansas at Little Rock, 2801 South University Avenue Little Rock, Arkansas 72204, USA
[3]Department of Chemistry, Guru Nanak Institutions Technical Campus (GNITC B-Tech-I), Ibrahimpatnam, Ranga Reddy, Hyderabad-501506, India
[4]Department of Chemistry, Government Junior College, Mustabad, Rajanna Sircilla-505404 India

*Corresponding authors: E-mail: satheeshkumar.n.9@gmail.com; ravinder@chaitanya.edu.in

Received: 2 August 2025 *Accepted*: 29 September 2025 *Published online*: 30 November 2025 AJC-22187

In this work, new hybrid compounds (**7a-o**) embedded with indole, thiazolidinedione and 1,2,3-triazole pharmacophores using Cu(I) catalyzed azide alkyne cycloaddition as key approach were synthesized and characterized. All these compounds were tested for their *in vitro* anticancer activity against three human cancer cell lines such as A549, MCF-7 and HeLa and nocodazole was used as reference drug. Compounds **7a**, **7c**, **7g**, **7l** and **7n** have shown predominant activity than nocodazole towards three cell lines with IC_{50} values ranging from 0.3 to 1.37 μM. These five potent compounds were further screened for *in vitro* tubulin polymerization inhibition assay, where compounds **7c**, **7g**, **7l** and **7n** exhibited more inhibition than the standard drug combretastatin A4 (CA-4). In *in silico* molecular docking studies all these five compounds displayed remarkable binding energies with target protein α,β-tubulin (PDB ID: 1SA0). Further, results of *in silico* ADMET of the same five compounds revealed that they followed Lipinski rule, Veber rule, Egan rule and Muegge rules without any deviation and lipophilicity (Log $P_{o/w}$) of the compounds was ranging from 2.80 to 4.06. Finally, compound **7n** was characterized using density functional theory (DFT) with B3LYP/6–311++G (d,p) basis set.

Keywords: Indole, Thiazolidinedione, 1,2,3-Triazole, Tubulin, Docking, ADMET, DFT.

INTRODUCTION

The indole core has consistently captured the attention of researchers, becoming a dynamic area of study due to its remarkable pharmacological properties [1-3]. It is often referred to as a privileged scaffold as it can bind to multiple receptors with high affinity, facilitating the development of novel bioactive drugs [4-8]. Indole is widely used in the target-based design and development of anticancer agents [9,10]. Especially many indole-based molecules act by interfering with tubulin polymerization which is a key component in cell division [11]. For example, vincristine and vinblastine (Fig. 1) are the two indole based vinca alkaloids available in nature which inhibit tubulin polymerization.

Thiazolidine-2,4-dione (TZD) has been recognized as a crucial structure in drug design and discovery [12,13]. A review of the literature shows that heterocyclic hybrids containing thiazolidine-2,4-dione exhibit various pharmacological activities [14-19]. Especially, several anticancer agents with the thiazolidine-2,4-dione core have been reported [20-24] and compounds like AZD1208 (Fig. 1), GSK1059615 and SMI-4a are currently undergoing clinical trials for cancer treatment [25-28].

The 1,2,3-triazole scaffold is widely recognized in drug discovery and development due to its diverse pharmacological activities, particularly its anticancer properties [29,30]. This is attributed to its ability to engage in hydrogen bonding, dipole-dipole interactions, hydrophobic interactions and van der Waals forces with target proteins in biological systems [31,32]. In this context, Vanaparthy *et al.* [33] synthesized a triazole hybrid molecule (A; Fig. 1) which inhibited tubulin polymerization at 0.22 μM concentration.

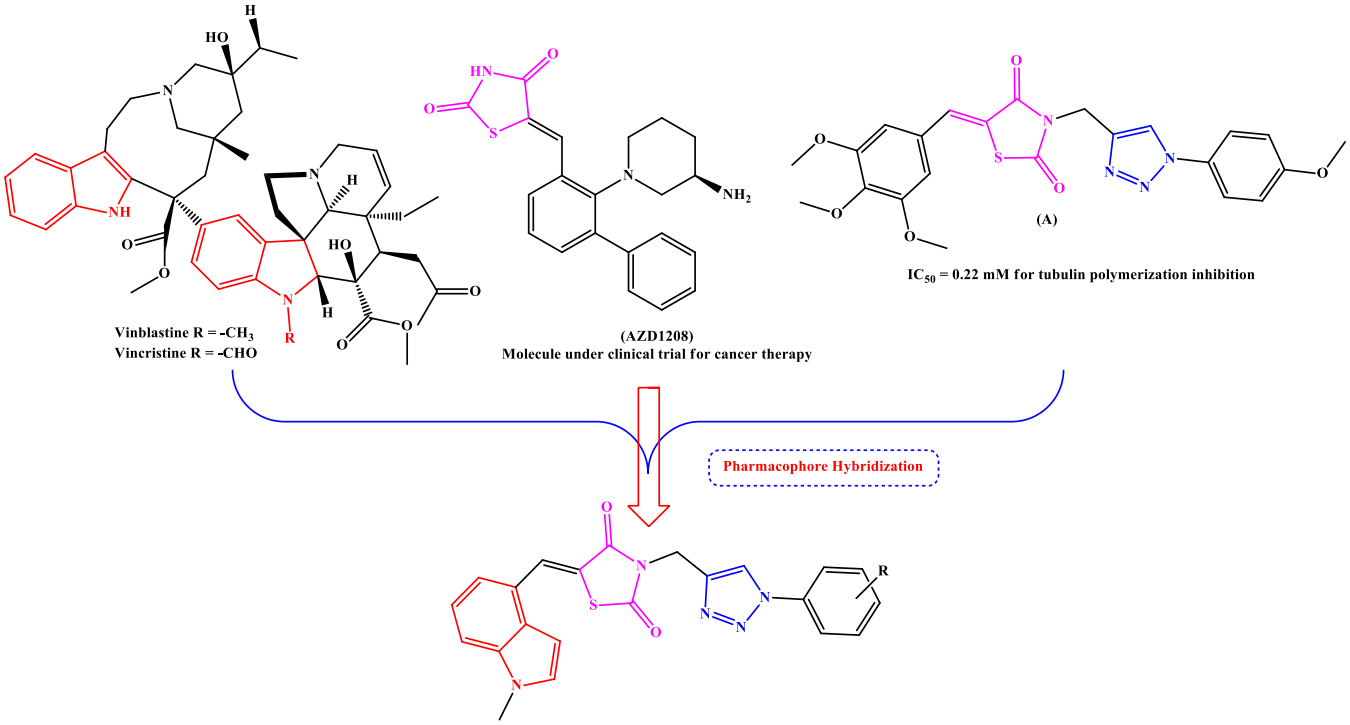

Fig. 1. Rationale and molecular design

Cancer is a leading cause of death worldwide, with current treatment options including surgery, chemotherapy, radiation therapy, or a combination of these approaches [34]. In recent decades, many heterocyclic compounds have been identified as potential anticancer agents [35,36]. Approximately 60% of the medications used in cancer treatment are based on heterocyclic structures [37]. While the prescribed doses of anticancer drugs are typically sufficient to kill cancer cells, they often cause harm to normal tissue and lead to various side effects, which limits their effectiveness [34]. As a result, researchers are actively seeking new anticancer drugs by designing and exploring novel compounds that can treat different types of cancer without the adverse effects associated with traditional antineoplastic therapies.

Tubulin is a key component of the cytoskeleton and plays a crucial role in cell mitosis, particularly during the G2/M phase. During the initial phase of mitosis, microtubules polymerize to form spindles, which help move sister chromatids toward the poles, facilitating cell division [38]. As a result, tubulin is considered a promising target for the development of new anticancer drugs [39]. Building on our ongoing research to develop novel biologically significant heterocycles [40-46] and considering the medicinal applications of indole, thiazolidine-2,4-dione and 1,2,3-triazole, we have designed the hybrid compounds as illustrated in Fig. 1. These compounds integrate the three pharmacophores by leveraging the pharmacophore hybridization approach [47,48].

EXPERIMENTAL

All commercially chemicals were utilized without further purification. The purity of all the chemicals was analyzed by Merck $60F_{254}$ silica gel TLC plates. Melting points calculated on a hot stage melting point apparatus, Ernst Leitz Wetzlar, Germany and uncorrected. The ^1H & ^{13}C NMR spectra were recorded by Mercuryplus spectrometer (400 MHz for ^1H & 100 MHz for ^{13}C) and chemical shifts referenced to TMS. ESI mass spectra at an ionising voltage of 70 eV attained using Shimadzu QP5050A quadrupole-mass spectrometer.

Synthesis of (Z)-5-((1-methyl-1*H*-indol-4-yl)methylene)-thiazolidine-2,4-dione (3): A mixture of 1-methyl-1*H*-indole-4-carbaldehyde (**1**) (0.025 mol), thiazolidine-2,4-dione (**2**) (0.025 mol) and piperidene (0.0025 mol) in EtOH (35 mL) was stirred at reflux for 22 h. The reaction mixture was then cooled for overnight and the obtained precipitate was filtered, washed with cold ethanol and dried. Finally, crude solid was crystallized from EtOH. Colourless solid; Yield: 53%; m.p.: 142-144 ºC; ^1H NMR (400 MHz, DMSO-d_6) δ ppm: 3.72 (s, 3H), **6**.53 (d, J = 7.3 Hz, 1H), 7.28 (d, J = 7.3 Hz, 1H), 7.41-7.46 (m, 3H), 7.68 (s, 1H), 12.87 (br s, 1H).

Synthesis of (Z)-5-((1-methyl-1*H*-indol-4-yl)methylene)-3-(prop-2-yn-1-yl)thiazolidine-2,4-dione (5): A mixture of compound **3** (0.012 mol), 3-bromoprop-1-yne (**4**) (0.016 mol) and Cs_2CO_3 (0.024 mol) in DMF (30 mL) was stirred at 100 ºC for 3 h. The completion of reaction as analyzed by TLC, excess of ice-cold water was added to reaction mixture. The obtained crude solid product was filtered and finally subjected to purification by 60-120 mesh size silica gel column chromatography using (1:4) ethyl acetate/hexane eluent. Colourless solid; Yield: 68%; m.p.: 146-148 ºC; ^1H NMR (400 MHz, DMSO-d_6) δ ppm: 2.32 (s, 1H), 3.71 (s, 3H), 4.39 (s, 2H), 6.73 (d, J = 7.3 Hz, 1H), 7.31 (d, J = 7.3 Hz, 1H), 7.43-7.48 (m, 3H), 7.67 (s, 1H).

General procedure for the synthesis of 1,2,3-triazole of indole-thiazolidine-2,4-dione (7a-o): A mixture of terminal alkyne **5** (0.5 mmol), aryl azides (**6a-o**) (1.0 mmol) and CuI (0.05 mmol) in THF (10 mL) was stirred at room temperature

for 17 h. The progress of reaction as monitored by TLC, reaction mixture extracted with ethyl acetate (2 × 15 mL), combined organic layer was dried under anhydrous Na_2SO_4 and evaporated under rotary evaporator (**Scheme-I**). The resulting crude products were purified by 60-120 mesh size silica gel column chromatography using (2:3) as ethyl acetate/hexane as mobile eluent.

(Z)-5-((1-Methyl-1*H*-indol-4-yl)methylene)-3-((1-phenyl-1*H*-1,2,3-triazol-4-yl)methyl)thiazolidine-2,4-dione (7a): Cream solid; yield: 74%; m.p.: 181-183 ºC; ^{1}H NMR (400 MHz, DMSO-d_6) δ ppm: 3.72 (s, 3H), 4.76 (s, 2H), 6.89 (d, *J* = 7.3 Hz, 1H), 7.35 (d, *J* = 7.3 Hz, 1H), 7.41-7.50 (m, 5H), 7.74 (s, 1H), 7.82-7.86 (m, 2H), 8.36 (s, 1H); ^{13}C NMR (100 MHz, DMSO-d_6) δ ppm: 36.6, 48.3, 103.5, 108.6, 116.3, 122.1, 123.1, 124.2, 125.3, 126.6, 128.1, 128.9, 129.8, 130.6, 134.7, 136.8, 138.2, 141.3, 166.3, 171.4 ppm; MS (ESI): *m/z* 350 $[M+H]^+$; CHN analysis for $C_{22}H_{17}N_5O_2S$; Calcd. (found) %: C, 63.60 (63.64); H, 4.12 (4.14); N, 16.86 (16.88).

(Z)-3-((1-(4-Methoxyphenyl)-1*H*-1,2,3-triazol-4-yl)-methyl)-5-((1-methyl-1*H*-indol-4-yl)methylene)thiazolidine-2,4-dione (7b): Colourless solid; yield: 69%; m.p.: 190-192 ºC; ^{1}H NMR (400 MHz, DMSO-d_6) δ ppm: 3.73 (s, 3H), 3.87 (s, 3H), 4.75 (s, 2H), 6.87 (d, *J* = 7.3 Hz, 1H), 6.95 (d, *J* = 7.4 Hz, 2H), 7.33 (d, *J* = 7.3 Hz, 1H), 7.42-7.47 (m, 3H), 7.58 (d, *J* = 7.4 Hz, 2H), 7.75 (s, 1H), 8.34 (s, 1H); ^{13}C NMR (100 MHz, DMSO-d_6) δ ppm: 36.7, 48.2, 56.7, 103.3, 108.7, 113.8, 116.4, 123.3, 123.9, 124.4, 125.4, 126.7, 128.8, 129.7, 132.3, 134.6, 136.8, 141.5, 158.3, 166.2, 171.3; MS (ESI): *m/z* 446 $[M+H]^+$; CHN analysis for $C_{23}H_{19}N_5O_3S$; Calcd. (found) %: C, 62.01 (62.03); H, 4.30 (4.33); N, 15.72 (15.68).

(Z)-3-((1-(3-Methoxyphenyl)-1*H*-1,2,3-triazol-4-yl)-methyl)-5-((1-methyl-1*H*-indol-4-yl)methylene)thiazolidine-2,4-dione (7c): Grey solid; yield: 70%; m.p.: 189-191 ºC; ^{1}H NMR (400 MHz, DMSO-d_6) δ ppm: 3.71 (s, 3H), 3.89 (s, 3H), 4.73 (s, 2H), 6.64-6.69 (m, 1H), 6.84-6.91 (m, 2H), 7.06 (t, *J* = 7.2 Hz, 1H), 7.15 (s, 1H), 7.31 (d, *J* = 7.3 Hz, 1H), 7.41-7.46 (m, 3H), 7.74 (s, 1H), 8.28 (s, 1H); ^{13}C NMR (100 MHz, DMSO-d_6) δ ppm: 36.8, 48.1, 56.9, 103.2, 106.4, 108.5, 113.5, 114.7, 116.3, 123.2, 124.3, 125.2, 126.8, 128.7, 129.6, 131.2, 134.7, 136.6, 139.7, 141.2, 160.7, 166.1, 171.2; MS (ESI): *m/z* 468 $[M+Na]^+$; CHN analysis for $C_{23}H_{19}N_5O_3S$; Calcd. (found) %: C, 62.01 (62.04); H, 4.30 (4.32); N, 15.72 (15.75).

(Z)-3-((1-(3,5-Dimethoxyphenyl)-1*H*-1,2,3-triazol-4-yl)methyl)-5-((1-methyl-1*H*-indol-4-yl)methylene)thiazolidine-2,4-dione (7d): Grey solid; yield: 65%; m.p.: 198-200 ºC; ^{1}H NMR (400 MHz, DMSO-d_6) δ ppm: 3.73 (s, 3H), 3.91 (s, 6H), 4.76 (s, 2H), 6.43 (s, 1H), 6.76 (s, 2H), 6.86 (d, *J* = 7.3 Hz, 1H), 7.32 (d, *J* = 7.3 Hz, 1H), 7.40-7.45 (m, 3H), 7.75 (s, 1H), 8.38 (s, 1H); ^{13}C NMR (100 MHz, DMSO-d_6) δ ppm: 36.5, 48.2, 56.8, 97.8, 99.7, 103.3, 108.7, 116.4, 123.3, 124.2, 125.4, 126.5, 128.8, 129.7, 134.5, 136.7, 140.6, 141.3, 160.8, 166.5, 171.4; MS (ESI): *m/z* 476 $[M+H]^+$; CHN analysis for $C_{24}H_{21}N_5O_4S$; Calculated (found) %: C, 60.62 (60.65); H, 4.45 (4.47); N, 14.73 (14.71).

(Z)-3-((1-(4-Methylphenyl)-1*H*-1,2,3-triazol-4-yl)-methyl)-5-((1-methyl-1*H*-indol-4-yl)methylene)thiazolidine-2,4-dione (7e): Colourless solid; yield: 74%; m.p.: 184-186 ºC; ^{1}H NMR (400 MHz, DMSO-d_6) δ ppm: 2.41 (s, 3H), 3.74 (s, 3H), 4.76 (s, 2H), 6.88 (d, *J* = 7.3 Hz, 1H), 7.31-7.36 (m, 3H), 7.41-7.46 (m, 3H), 7.71-7.76 (m, 3H), 8.35 (s, 1H); ^{13}C NMR (100 MHz, DMSO-d_6) δ ppm: 21.7, 36.8, 48.3, 103.2, 108.5, 116.5, 123.2, 124.4, 124.9, 125.3, 126.7, 128.7, 129.8, 130.4, 134.6, 136.6, 137.6, 138.5, 141.5, 166.4, 171.4; MS (ESI): *m/z* 430 $[M+H]^+$; CHN analysis for $C_{23}H_{19}N_5O_2S$; Calcd. (found) %: C, 64.32 (64.34); H, 4.46 (4.49); N, 16.31 (16.33).

(Z)-3-((1-(3-Methylphenyl)-1*H*-1,2,3-triazol-4-yl)-methyl)-5-((1-methyl-1*H*-indol-4-yl)methylene)thiazolidine-2,4-dione (7f): Light yellow solid; yield: 72%; m.p.: 185-187 ºC; ^{1}H NMR (400 MHz, DMSO-d_6) δ ppm: 2.43 (s, 3H), 3.73 (s, 3H), 4.75 (s, 2H), 6.86 (d, *J* = 7.3 Hz, 1H), 6.91-6.96 (m,

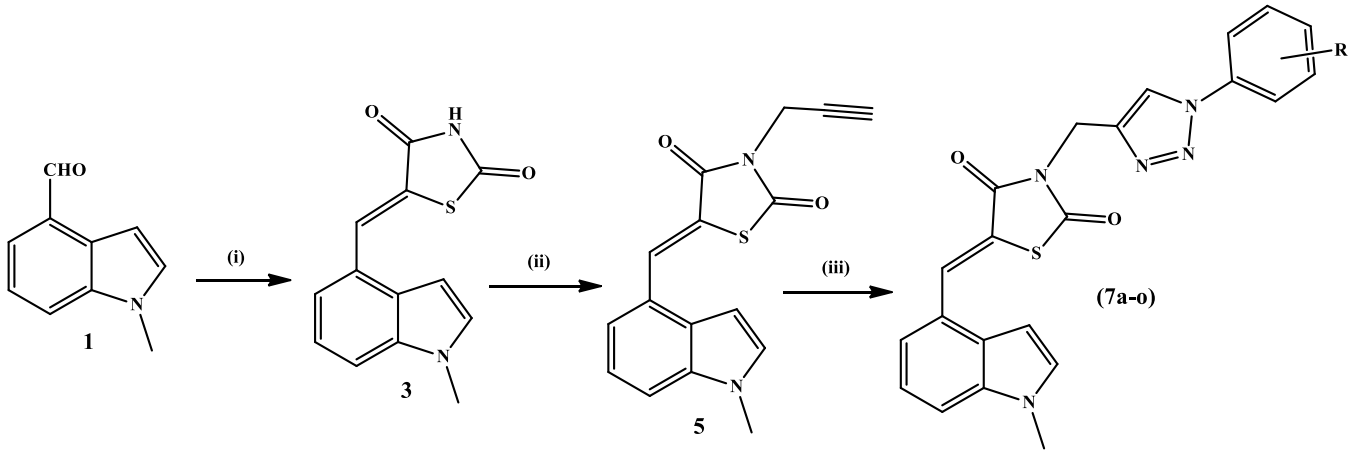

R = H; 7a; 74%; R = 4-OMe; 7b; 69%; R = 3-OMe; 7c; 70%; R = 3,5-diOMe; 7d; 65%; R = 4-Me; 7e; 74%; R = 3-Me; 7f; 72%; R = 3,5-diMe; 7g; 70%; R = 4-Br; 7h; 75%; R = 4-F; 7i; 78%; R = 4-Cl; 7j; 77%; R = 3-Cl; 78%;7k; R = 3,5-diCl; 7l; 76%; R = 4-NO_2; 7m; 80%; R = 4-CN; 7n; 77%; R = 4-$COCH_3$; 7o; 79%

Reaction conditions:

(i) Thiazolidine-2,4-dione (2), piperidine, EtOH, reflux, 22 h.

(ii) 3-bromoprop-1-yne (4), Cs_2CO_3, DMF, 100 ºC, 3 h.

(ii) Ar-N_3 (6a-6o), CuI, THF, RT, 18 h.

Scheme-I: Synthesis of indole-thiazolidinedione-1,2,3-triazole conjugates (**7a-o**)

1H), 7.20 (t, *J* = 7.8 Hz, 1H), 7.30-7.34 (m, 2H), 7.37-7.45 (m, 4H), 7.73 (s, 1H), 8.37 (s, 1H); ^{13}C NMR (100 MHz, DMSO-d_6) δ ppm: 21.9, 36.6, 48.1, 103.5, 108.7, 116.4, 117.6, 123.3, 124.2, 124.9, 125.5, 126.1, 126.8, 128.1, 128.7, 129.6, 134.5, 136.8, 139.3, 140.2, 141.3, 166.3, 171.2; MS (ESI): *m/z* 452 $[M+Na]^+$; CHN analysis for $C_{23}H_{19}N_5O_2S$; Calcd. (found) %: C, 64.32 (64.36); H, 4.46 (4.49); N, 16.31 (16.33).

(*Z*)-3-((1-(3,5-Dimethylphenyl)-1*H*-1,2,3-triazol-4-yl)-methyl)-5-((1-methyl-1*H*-indol-4-yl)methylene)thiazolidine-2,4-dione (7g): Colourless solid; yield: 70%; m.p.: 191-193 ºC; ^{1}H NMR (400 MHz, DMSO-d_6) δ ppm: 2.43 (s, 6H), 3.74 (s, 3H), 4.75 (s, 2H), 6.87 (d, *J* = 7.3 Hz, 1H), 7.05 (s, 1H), 7.32 (d, *J* = 7.3 Hz, 1H), 7.40-7.45 (m, 3H), 7.51 (s, 2H), 7.75 (s, 1H), 8.28 (s, 1H); ^{13}C NMR (100 MHz, DMSO-d_6) δ ppm: 21.8, 36.8, 48.4, 103.6, 108.8, 116.5, 123.2, 124.4, 125.3, 125.8, 126.5, 127.3, 128.8, 129.9, 134.7, 136.6, 138.6, 140.2, 141.4, 166.3, 171.4; MS (ESI): *m/z* 444 $[M+H]^+$; CHN analysis for $C_{24}H_{21}N_5O_2S$; Calcd. (found) %: C, 64.99 (64.97); H, 4.77 (4.74); N, 15.79 (15.82).

(*Z*)-3-((1-(4-Bromophenyl)-1*H*-1,2,3-triazol-4-yl)-methyl)-5-((1-methyl-1*H*-indol-4-yl)methylene)thiazolidine-2,4-dione (7h): Light orange solid; yield: 75%; m.p.: 217-219 ºC; ^{1}H NMR (400 MHz, DMSO-d_6) δ ppm: 3.72 (s, 3H), 4.77 (s, 2H), 6.88 (d, *J* = 7.3 Hz, 1H), 7.34 (d, *J* = 7.3 Hz, 1H), 7.40-7.48 (m, 5H), 7.73 (s, 1H), 7.83 (d, *J* = 7.8 Hz, 2H), 8.34 (s, 1H); ^{13}C NMR (100 MHz, DMSO-d_6) δ ppm: 36.5, 48.1, 103.5, 108.7, 116.4, 120.9, 122.3, 123.3, 124.5, 125.2, 126.6, 128.6, 129.7, 132.8, 134.5, 135.9, 136.7, 141.3, 166.4, 171.3; MS (ESI): *m/z* 494 $[M+H]^+$; CHN analysis for $C_{22}H_{16}BrN_5O_2S$; Calcd. (found) %: C, 53.45 (53.47); H, 3.26 (3.29); N, 14.17 (14.20).

(Z)-3-((1-(4-Fluorophenyl)-1*H*-1,2,3-triazol-4-yl)-methyl)-5-((1-methyl-1*H*-indol-4-yl)methylene)thiazolidine-2,4-dione (7i): Cream solid; yield: 78%; m.p.: 184-186 ºC; ^{1}H NMR (400 MHz, DMSO-d_6) δ ppm: 3.74 (s, 3H), 4.79 (s, 2H), 6.85 (d, *J* = 7.3 Hz, 1H), 7.11 (d, *J* = 7.1 Hz, 2H), 7.31 (d, *J* = 7.3 Hz, 1H), 7.39-7.44 (m, 3H), 7.54 (d, *J* = 7.1 Hz, 2H), 7.75 (s, 1H), 8.36 (s, 1H); 36.8, 48.3, 103.6, 108.8, 116.5, 118.3, 123.2, 123.8, 124.4, 125.3, 126.5, 128.8, 129.9, 134.1, 134.7, 136.9, 141.5, 160.3, 166.2, 171.3; ^{13}C NMR (100 MHz, DMSO-d_6) δ ppm: MS (ESI): *m/z* 434 $[M+H]^+$; CHN analysis for $C_{22}H_{16}FN_5O_2S$; Calcd. (found) %: C, 60.96 (60.93); H, 3.72 (3.76); N, 16.16 (16.18).

(*Z*)-3-((1-(4-Chlorophenyl)-1*H*-1,2,3-triazol-4-yl)-methyl)-5-((1-methyl-1*H*-indol-4-yl)methylene)thiazolidine-2,4-dione (7j): Colourless solid; yield:77%; m.p.: 189-191 ºC; ^{1}H NMR (400 MHz, DMSO-d_6) δ ppm: 3.73 (s, 3H), 4.77 (s, 2H), 6.87 (d, *J* = 7.3 Hz, 1H), 7.31-7.36 (m, 3H), 7.40-7.45 (m, 3H), 7.70-7.75 (m, 3H), 8.34 (s, 1H); ^{13}C NMR (100 MHz, DMSO-d_6) δ ppm: 36.7, 48.1, 103.4, 108.5, 116.4, 123.3, 123.8, 124.2, 125.4, 126.7, 128.7, 129.6, 130.2, 133.1, 134.6, 136.7, 137.3, 141.3, 166.5, 171.5; MS (ESI): *m/z* 450 $[M+H]^+$; CHN analysis for $C_{22}H_{16}ClN_5O_2S$; Calcd. (found) %: C, 58.73 (58.75); H, 3.58 (3.61); N, 15.57 (15.59).

(*Z*)-3-((1-(3-Chlorophenyl)-1*H*-1,2,3-triazol-4-yl)-methyl)-5-((1-methyl-1*H*-indol-4-yl)methylene)thiazolidine-2,4-dione (7k): Colourless solid; yield: 78%; m.p.: 188-190 ºC; ^{1}H NMR (400 MHz, DMSO-d_6) δ ppm: 3.74 (s, 3H), 4.76 (s, 2H), 6.86 (d, *J* = 7.3 Hz, 1H), 7.08-7.13 (m, 1H), 7.19 (t, *J* = 7.5 Hz, 1H), 7.30-7.35 (m, 2H), 7.41-7.46 (m, 3H), 7.67 (s, 1H), 7.74 (s, 1H), 8.32 (s, 1H); ^{13}C NMR (100 MHz, DMSO-d_6) δ ppm: 36.8, 48.2, 103.6, 108.7, 116.3, 119.1, 122.1, 123.2, 124.3, 125.5, 126.1, 126.8, 128.9, 129.9, 130.7, 134.5, 135.1, 136.6, 140.3, 141.5, 166.2, 171.4; MS (ESI): *m/z* 450 $[M+H]^+$; CHN analysis for $C_{22}H_{16}ClN_5O_2S$; Calcd. (found) %: C, 58.73 (58.76); H, 3.58 (3.54); N, 15.57 (15.59).

(*Z*)-3-((1-(3,5-Dichlorophenyl)-1*H*-1,2,3-triazol-4-yl)-methyl)-5-((1-methyl-1*H*-indol-4-yl)methylene)thiazolidine-2,4-dione (7l): Grey solid; yield: 76%; m.p.: 193-195 ºC; ^{1}H NMR (400 MHz, DMSO-d_6) δ ppm: 3.72 (s, 3H), 4.78 (s, 2H), 6.88 (d, *J* = 7.3 Hz, 1H), 7.24 (s, 1H), 7.32 (d, *J* = 7.3 Hz, 1H), 7.39-7.44 (m, 3H), 7.56 (s, 2H), 7.73 (s, 1H), 8.37 (s, 1H); ^{13}C NMR (100 MHz, DMSO-d_6) δ ppm: 36.5, 48.4, 103.4, 108.6, 116.4, 119.1, 123.3, 124.5, 124.9, 125.4, 126.7, 128.8, 129.7, 134.6, 135.9, 136.8, 139.8, 141.3, 166.5, 171.6; MS (ESI): *m/z* 485 $[M+H]^+$; CHN analysis for $C_{22}H_{15}Cl_2N_5O_2S$; Calcd. (found) %: C, 54.56 (54.53); H, 3.12 (3.16); N, 14.46 (14.44).

(*Z*)-5-((1-Methyl-1*H*-indol-4-yl)methylene)-3-((1-(4-nitrophenyl)-1*H*-1,2,3-triazol-4-yl)methyl)thiazolidine-2,4-dione (7m): Light yellow solid; yield: 80%; m.p.: 197-199 ºC; ^{1}H NMR (400 MHz, DMSO-d_6) δ ppm: 3.74 (s, 3H), 4.76 (s, 2H), 6.89 (d, *J* = 7.3 Hz, 1H), 7.35 (d, *J* = 7.3 Hz, 1H), 7.41-7.46 (m, 3H), 7.76 (s, 1H), 7.82 (d, *J* = 7.2 Hz, 2H), 8.19 (d, *J* = 7.2 Hz, 2H), 8.36 (s, 1H); ^{13}C NMR (100 MHz, DMSO-d_6) δ ppm: 36.7, 48.1, 103.6, 108.7, 116.2, 122.9, 123.2, 124.4, 125.5, 126.8, 127.5, 128.9, 129.7, 134.5, 136.7, 141.5, 142.1, 148.3, 166.4, 171.6; MS (ESI): *m/z* 350 $[M+H]^+$; CHN analysis for $C_{22}H_{16}N_6O_4S$; Calcd. (found) %: C, 57.39 (57.41); H, 3.50 (3.47); N, 18.25 (18.29).

(Z)-4-(4-((5-((1-Methyl-1*H*-indol-4-yl)methylene)-2,4-dioxothiazolidin-3-yl)methyl)-1*H*-1,2,3-triazol-1-yl)benzonitrile (7n): Light orange solid; yield: 77%; m.p.: 187-189 ºC; ^{1}H NMR (400 MHz, DMSO-d_6) δ ppm: 3.73 (s, 3H), 4.77 (s, 2H), 6.87 (d, *J* = 7.3 Hz, 1H), 7.33 (d, *J* = 7.3 Hz, 1H), 7.41-7.46 (m, 3H), 7.52 (d, *J* = 8.1 Hz, 2H), 7.74 (s, 1H), 7.86 (d, *J* = 8.1 Hz, 2H), 8.37 (s, 1H); ^{13}C NMR (100 MHz, DMSO-d_6) δ ppm: 36.8, 48.4, 103.5, 108.8, 116.3, 117.6, 119.8, 123.3, 124.5, 125.4, 126.1, 126.7, 127.6, 128.7, 129.8, 134.6, 136.8, 140.2, 141.3, 166.2, 171.3; MS (ESI): *m/z* 350 $[M+H]^+$; CHN analysis for $C_{23}H_{16}N_6O_2S$; Calcd. (found) %: C, 62.72 (62.70); H, 3.66 (3.69); N, 19.08 (19.06).

(*Z*)-3-((1-(4-Acetylphenyl)-1*H*-1,2,3-triazol-4-yl)methyl)-5-((1-methyl-1*H*-indol-4-yl)methylene)thiazolidine-2,4-dione (7o): Light yellow solid; yield: 79%; m.p.: 193-195 ºC; ^{1}H NMR (400 MHz, DMSO-d_6) δ ppm: 2.56 (s, 3H), 3.75 (s, 3H), 4.76 (s, 2H), 6.85 (d, *J* = 7.3 Hz, 1H), 7.32 (d, *J* = 7.3 Hz, 1H), 7.40-7.45 (m, 3H), 7.64-7.68 (m, 4H), 7.73 (s, 1H), 8.31 (s, 1H); ^{13}C NMR (100 MHz, DMSO-d_6) δ ppm: 28.7, 36.7, 48.2, 103.6, 108.7, 116.4, 123.4, 123.9, 124.4, 124.8, 125.5, 126.8, 128.8, 129.9, 133.5, 134.5, 136.7, 139.5, 141.6, 166.5, 171.7, 196.8; MS (ESI): *m/z* 350 $[M+H]^+$; CHN analysis for $C_{24}H_{19}N_5O_3S$; Calcd. (found) %: C, 63.01 (63.05); H, 4.19 (4.17); N, 15.31 (15.35).

MTT assay: Individual wells of 96-well tissue culture microtiter plates were seeded with 100 μL of complete medium containing 1×10^4 cells. The plates were incubated at 37 ºC in a humidified atmosphere with 5% CO_2 for 18 h prior to the

experiment. Following medium removal, 100 µL of fresh medium containing the test compounds and nocodazole at concentrations of 0.5, 1 and 2 µM were added to each well and the plates were incubated at 37 ºC for 24 h. After incubation, the medium was discarded and 10 µL of MTT dye solution was added to each well. The plates were incubated at 37 ºC for 2 h to allow for formazan crystal formation. The crystals were then solubilized in 100 µL of extraction buffer and the optical density (OD) was measured at 570 nm using a Multi-mode Varioskan microplate reader (Thermo-Scientific). The final DMSO concentration in the medium did not exceed 0.25%.

***in vitro* Tubulin polymerization inhibition:** Tubulin polymerization inhibitory activity was assessed using a commercial kit (Cytoskeleton, cat. #BK011P) following the manufacturer's instructions. The assay utilized tubulin isolated from porcine brain tissue. A tubulin reaction mixture was prepared containing 2.0 mM $MgCl_2$, 0.5 mM EGTA, 80.0 mM PIPES (pH 6.9), 1 mM GTP and 10.2% glycerol. Subsequently, 5 µL of the test compounds at the specified concentrations were added to the mixture, which was pre-warmed to 37 ºC for 1 min. The reaction was initiated by adding 55 µL of tubulin solution. Fluorescence intensity was measured every 60 s for 90 min using a multifunction microplate reader. The IC_{50} value was determined based on the area under the curve.

Molecular docking: Molecular docking studies were performed using AutoDock 4.2. The protein structure (PDB ID: 1SA0) was obtained from the Protein Data Bank. Ligands and water molecules were removed from the protein and Gasteiger charges were calculated after adding polar hydrogens. Ligands were drawn using ChemDraw 12, saved as. mol files and subjected to energy minimization. These were then converted to PDB files using Discovery Studio. A grid box was generated with 60 points along each of the three coordinate axes. The Lamarckian Genetic Algorithm (LGA) in AutoDock 4.2 was employed to generate the .dpf file. The .dlg file was obtained using the Cygwin interface, from which the docking results were extracted. 2D and 3D visualizations were created using Schrödinger's Maestro v9.5.

DFT studies: In computational methods, Gaussian 09 software program package was used. The quantum chemical calculations were performed by the density functional theory method with the three-parameter hybrid functional (B3) for the exchange part and the Lee-Yang-Par (LYP) correlation function with B3LYP/6-311G++ (d,p) basis set. The structural parameters were derived from geometry optimization and molecular electrostatic potential (MEP), which summarizes the charge distribution of the molecule was examined to find out the nucleophilic and electrophilic regions of the molecule, visualization program is utilized to view the shape of HOMO-LUMO. Moreover, the energy distribution of the molecular orbitals and the HOMO-LUMO energy gap was calculated.

RESULTS AND DISCUSSION

The synthesis of targeted 1,2,3-triazoles of indole-thiazolidine-2,4-dione (**7a-o**) was achieved successfully in three steps (**Scheme-I**). First step involves the Knoevenagel condensation of 1-methyl-1*H*-indole-4-carbaldehyde (**1**) with thiazolidine-2,4-dione (**2**) in the presence of piperidene catalyst in ethanol by refluxing for 22 h to obtain (Z)-5-((1-methyl-1*H*-indol-4-yl)methylene)thiazolidine-2,4-dione (**3**). In ^{1}H NMR spectrum, the existence of new broad singlet signal at δ value 12.87 ppm confirms the Knoevenagel product. In second step, the Knoevenagel compound (**3**) was treated with 3-bromo-prop-1-yne (**4**) in the presence of Cs_2CO_3 in DMF at 100 ºC for 3 h to afford (*Z*)-5-((1-methyl-1*H*-indol-4-yl)methylene)-3-(prop-2-yn-1-yl)thiazolidine-2,4-dione (**5**). In ^{1}H NMR spectrum, the absence of broad singlet signal at δ value 12.87 ppm and existence of new singlet signals at δ values 4.34 and 2.32 ppm respectively support the formation of terminal alkyne (**5**). Finally, CuI-catalzyed [3+2] cycloaddition between terminal alkyne **5** and aryl azides (**6a-o**) at ambient temperature in THF for 17 h gave new anticipated 1,4-disubstituted 1,2,3-triazoles (**7a-o**) in moderate to good yields. The structures of final compounds (**7a-o**) characterized by ^{1}H NMR, ^{13}C NMR Mass spectra and CHN analysis. For a representative compound **7a**, in ^{1}H NMR spectrum, the presence of new singlet signal at δ value 8.36 ppm supports the formation of 1,2,3-triazole ring. Similarly, in ^{13}C NMR spectrum formation of new peak at δ value 124.2 ppm further supports the formation of 1,2,3-triazole ring.

***In vitro* anticancer activity:** The cytotoxicity of all newly synthesized 1,2,3-triazoles was tested against three human cancer cell lines like A549, MCF-7 and HeLa using the MTT assay, with nocodazole serving as the standard drug. Table-1 showed that compounds **7a**, **7c**, **7g**, **7l** and **7h** demonstrated higher activity against all three cell lines compared to nocodazole. In particular, compound **7n** has displayed highest activity among all the compounds against the A549, MCF-7 and HeLa cell lines with IC_{50} values 0.3, 0.8 and 1.1 µM, respectively. Further compound **7c** exhibited second highest activity with IC_{50} values ranging from 0.5 to 1.2 µM.

TABLE-1
In vitro CYTOTOXICITY OF NEWLY SYNTHESIZED COMPOUNDS (**7a-o**) WITH [a]IC_{50} (µM)

Compound	[b]A549	[c]MCF-7	[d]HeLa
7a	0.9 ± 0.01	1.29 ± 0.01	1.37 ± 0.02
7b	15.27 ± 0.86	25.54 ± 1.12	38.74 ± 1.22
7c	0.5 ± 0.01	0.9 ± 0.01	1.2 ± 0.02
7d	25.77 ± 1.25	45.14 ± 1.20	28.14 ± 1.18
7e	23.47 ± 1.20	34.24 ± 1.19	31.28 ± 1.51
7f	41.62 ± 1.41	51.34 ± 1.27	64.47 ± 1.84
7g	0.6 ± 0.01	1.1 ± 0.01	1.2 ± 0.01
7h	71.82 ± 1.91	87.34 ± 1.95	77.47 ± 1.95
7i	31.40 ± 1.45	54.14 ± 1.67	47.80 ± 1.54
7j	54.17 ± 1.81	67.27 ± 1.85	74.27 ± 1.58
7k	81.27 ± 1.27	45.68 ± 1.25	34.14 ± 1.30
7l	0.8 ± 0.01	1.2 ± 0.01	1.3 ± 0.02
7m	83.27 ± 1.41	74.17 ± 1.45	96.17 ± 1.90
7n	0.3 ± 0.01	0.8 ± 0.01	1.1 ± 0.02
7o	48.41 ± 1.58	56.48 ± 1.55	52.58 ± 1.24
Nocodazole	1.0 ± 0.01	1.35 ± 0.02	1.41 ± 0.02

NI = IC_{50} > 100 µM; [a]Each data represents as mean ± S.D values; [b]A549: Human lung cancer cell line; [c]MCF-7: Human breast cancer cell line; [d]HeLa: Human cervix cancer cell line.

The structure-activity relationships (SARs) were established based on the IC_{50} data presented in Table-1. First, for

compounds containing electron-donating groups, compound **7c** having methoxy substituent at 3rd position has displayed highest activity and compound **7g** having methyl groups at 3rd and 5th positions ranked second in this series. Further the compound **7a** without any substituent has exhibited greater activity than nocodazole, standard. Compounds **7b** and **7d** having 4-methoxy and 3,5-dimethoxy substituents have shown less activity than compound **7c**. Similarly, compounds **7e** and **7f** having 4-methyl and 3-mehtyl groups also exhibited less activity than compound **7g**. On the other hand, in case of compounds with electron withdrawing groups the compound **7n** with nitrile group at 4th position has exhibited highest among all the fifteen compounds. Furthermore, compound **7l** with two chlorine atoms at 3rd and 5th positions has displayed second highest activity in this series. In the case of monohalogenated compounds the activity order was found to be 4-F > 4-Cl > 4-Br > 3-Cl for A549 cell line, 3-Cl > 4-F > 4-Cl > 4-Br for both MCF-7 and HeLa cell lines. Compound **7o** with acetyl group at 4th position exhibited less activity than compounds **7i** and **7k**. Finally, compound **7m**, with a 4-nitro substituent, exhibited lowest activity in the entire series.

***in vitro* Tubulin polymerization inhibitory activity:** Compounds **7a**, **7c**, **7g**, **7l** and **7n** were additionally tested for the tubulin polymerization inhibitory activity using previously described method, with combretastatin A4 (CA-4) serving as standard [49]. According to Table-2, compound **7n** has shown four times greater inhibitory potency than standard CA-4 with IC_{50} equal to 0.25 μM. Similarly, compound **7c** has shown nearly three times more inhibition than CA-4 with IC_{50} equal to 0.37 μM. Further, compounds **7g** and **7l** were also exhibited significant inhibition in comparison to CA-4. Finally, compound **7a** has shown less activity with IC_{50} equal to 2.94 μM.

TABLE-2
TUBULIN POLYMERIZATION INHIBITORY ACTIVITY

Compound	IC_{50} (μM)[a]
7a	2.94 ± 0.02
7c	0.37 ± 0.01
7g	0.74 ± 0.02
7l	0.48 ± 0.02
7n	0.25 ± 0.01
CA-4	1.10 ± 0.01

[a]The values are indicated as the mean ± SD.

Molecular docking studies: Compounds **7a**, **7c**, **7g**, **7l** and **7n**, which were exhibited higher *in vitro* anticancer activity were screened for their binding interactions with α,β-tubulin protein [50] using Auto Dock tools and combretastatin A-4 was used as reference. In this study, the compound **7n** having 4-nitril substituent has exhibited greatest binding energy *i.e.* -9.81 kcal/mol (Table-3). The inhibition constant of the same compound was found to be 64.65 nM. The nitrogen of nitrile group has formed one hydrogen bond with GLN96 residue with bond length 2.17 Å and oxygen atom of thiazolidine-dione has formed one hydrogen bond with LYS163 amino acid having bond length 2.26 Å (Fig. 2). Compound **7c** has exhibited second highest binding interactions with target protein

TABLE-3
MOLECULAR DOCKING INTERACTIONS OF COMPOUNDS **7a**, **7c**, **7g**, **7l** AND **7n** WITH α,β-TUBULIN (PDB ID: 1SA0)

Compd.	Binding energy (kcal/mol)	Inhibition constant	Number of hydrogen bonds	Residues involved in hydrogen bonding (bond length in Å)
7a	-9.07	224.95 nM	1	SER178(2.30)
7c	-9.62	88.50 nM	4	ARG2(1.98), LYS163(2.64), LYS164(1.96), SER165(1.87)
7g	-9.43	121.85 nM	3	LYS163(2.53), LYS164(1.98), SER165(2.09)
7l	-9.11	211.31 nM	3	LYS163(2.60), LYS164(1.92), SER165(1.95)
7n	-9.81	64.65 nM	2	LYS163(2.26), GLN96(2.17)
CA-4	-6.76	11.09 μM	2	VAL353(2.20), ILE355(1.86)

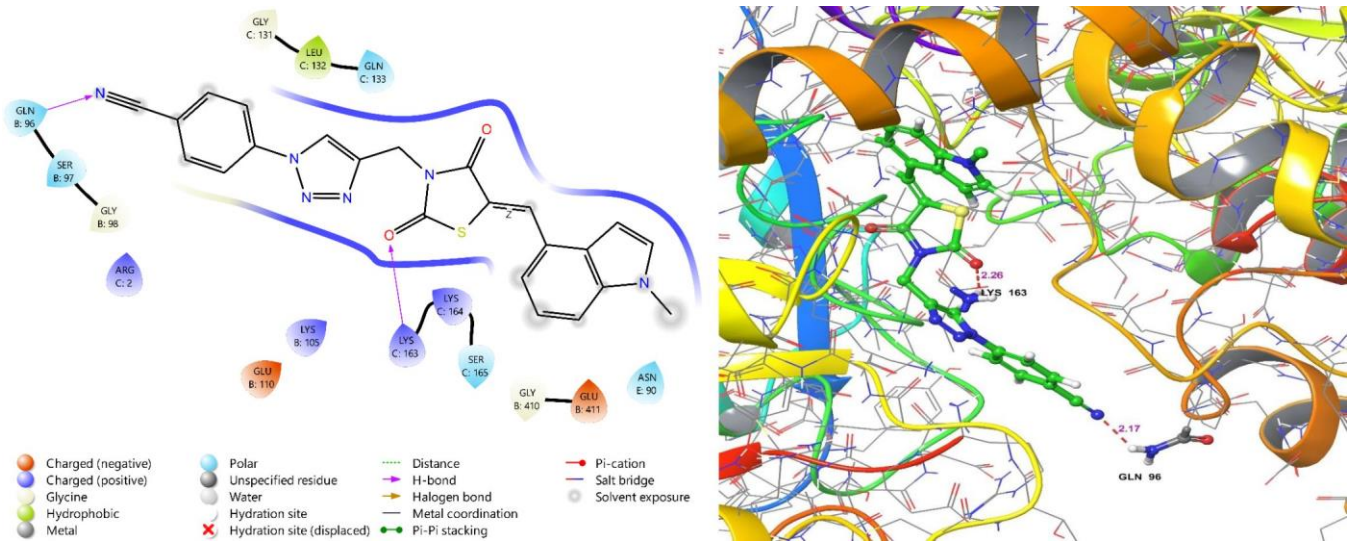

Fig. 2. 2D and 3D interaction of the compound with α,β-tubulin

with -9.62 kcal/mol, binding energy and it has formed four hydrogen bonds with ARG2, LYS163, LYS164 and SER165 residues with bond lengths 1.98 Å, 2.64 Å, 1.96 Å and 1.87 Å, respectively. Similarly, compound **7g** with two methyl groups at 3rd and 5th positions has exhibited significant binding energy (-9.43 kcal/mol) and inhibition constant (121.85 nM) with the target protein. It also formed three hydrogen bonds with LYS163 (bond length; 2.53 Å), LYS164 (bond length; 1.98 Å), SER165 (bond length; 2.09 Å) residues. Further, compounds **7a** and **7l** have shown almost similar binding energies (-9.07 kcal/mol and -9.11 kcal/mol, respectively) with α,β-tubulin. The oxygen atom of thiazolidinedione of compound **7a** has formed a hydrogen bond with SER178 residue with bond length 2.30 Å. Further, it has exhibited π-π stacking with TYR224 residue. Compound **7l** has formed three hydrogen bonds with LYS163 (bond length; 2.60 Å), LYS164 (bond length; 1.92 Å) and SER165 (bond length; 1.95 Å). The reference combretastatin A-4 also docked with α,β-tubulin where it has exhibited -6.76 kcal/mol, binding energy and also formed two hydrogen bonds with ILE355 (bond length 1.86 Å) and VAL353 (bond length 2.20 Å).

***in silico* Pharmacokinetic profile (ADMET):** The selected five compounds **7a**, **7c**, **7g**, **7l** and **7n**, identified as the most active based on their *in vitro* anticancer potency and ability to inhibit tubulin polymerization, were further analyzed for their pharmacokinetic and drug-likeness properties using the *in silico* tools pkCSM [51] and SwissADME [52]. According to the results, all the five compounds have less water solubility (log S parameter; Table-4). They have exhibited positive Caco2 permeability (log Papp in 10^{-6} cm/s), volume of distribution (log L/kg) and fraction unbound. But all of them were displayed negative CNS permeability (log PS) and blood-brain barrier permeability (log BB). In case of metabolism, all the compounds interacted with CYP3A4 (cytochrome P450). In addition, they inhibited CYP2C19 and CYP2C9. The compounds **7a**, **7c** and **7g** have inhibited CYP1A2 also. The excretion (log value of mL/min/kg) of the compounds **7a**, **7c**, **7g**, **7l** and **7n** found to be 0.13, 0.288, -0.082, 0.043 and 0.097 respectively. In case of toxicity prediction, all the compounds except **7l** have shown hepatotoxicity (Table-5). Further, all of them inhibited hERG II. All compounds inactive towards hERG I inhibition. Similarly, none of the compounds have shown skin permeation and AMES toxicity. The maximum tolerated dose (human; expressed in log value of mg/kg/day) of the compounds **7a**, **7c**, **7g**, **7l** and **7n** was 0.383, 0.356, 0.17, 0.209 and 0.184 respectively. All the five compounds have followed Lipinski rule, Veber rule, Egan rule and Muegge rules without any deviation. However, compounds **7g** and **7l** not followed Ghose rule because of more molar refractivity (Table-6). The lipophilicity (Log $P_{o/w}$) of compounds **7a**, **7c**,

TABLE-4
CALCULATION OF ADME PROPERTIES OF COMPOUNDS **7a**, **7c**, **7g, 7l** AND **7n** USING pkCSM

Compd.	Absorption			Distribution				Metabolism (S=Substrate; I=Inhibitor)	Excretion Log (mL/min/kg)
	Log S (log mol/L)	Caco2 perm. (log Papp in 10^{-6} cm/s)	Int. abs. (% abs.)	VDss (Log L/kg)	Fract. unb. (Fu)	BBB perm. (log BB)	CNS perm. (log PS)		
7a	-4.196	1.209	94.334	0.154	0.041	-0.878	-2.146	CYP3A4 (S & I) CYP1A2 (I) CYP2C19 (I) CYP2C9 (I)	0.13
7c	-4.307	1.272	95.541	0.116	0.021	-1.096	-2.307	CYP3A4 (S & I) CYP1A2 (I) CYP2C19 (I) CYP2C9 (I)	0.288
7g	-4.469	1.245	94.984	0.253	0.057	-0.877	-1.988	CYP3A4 (S & I) CYP1A2 (I) CYP2C19 (I) CYP2C9 (I)	-0.082
7l	-4.693	1.225	92.067	0.205	0.039	-1.227	-1.907	CYP3A4 (S & I) CYP2C19 (I) CYP2C9 (I)	0.043
7n	-4.177	0.672	95.657	0.143	0.037	-1.057	-2.2	CYP3A4 (S & I) CYP2C19 (I) CYP2C9 (I)	0.097

TABLE-5
TOXICITY PREDICTION OF COMPOUNDS **7a, 7c, 7g, 7l** AND **7n** USING pkCSM

Compd.	AMES toxicity	hERG I inhibitor	hERG II inhibitor	Hepatotoxicity	Skin permeation	Max. tolerated dose (human); log (mg/kg/day)
7a	No	No	Yes	Yes	No	0.383
7c	No	No	Yes	Yes	No	0.356
7g	No	No	Yes	Yes	No	0.170
7l	No	No	Yes	No	No	0.209
7n	No	No	Yes	Yes	No	0.184

TABLE-6
DRUG LIKENESS AND LIPOPHILICITY PROFILE OF THE COMPOUNDS **7a**, **7c**, **7g, 7l** AND **7n** CALCULATED USING SWISS/ADME

Compd.	Lipinski rule	Ghose rule	Veber rule	Egan rule	Muegge rule	Lipophilicity (Log $P_{o/w}$)
7a	Yes	Yes	Yes	Yes	Yes	2.99
7c	Yes	Yes	Yes	Yes	Yes	3.01
7g	Yes	No; 1 violation: MR > 130	Yes	Yes	Yes	3.69
7l	Yes	No; 2 violations: MW > 480, MR > 130	Yes	Yes	Yes	4.06
7n	Yes	Yes	Yes	Yes	Yes	2.80

7g, **7l** and **7n** was found to be 2.99, 3.01, 3.69, 4.06 and 2.80, respectively.

DFT studies

Molecular geometry: The molecular structure and atom numbering of compound **7n** are shown in Fig. 3. This molecule contains 21 C–C bond lengths, 9 C–N bond lengths, 2 N–N bond lengths, 2 C–O bond lengths and 2 C–S bond lengths. From the structural data provided in Table-7, it can be observed that C47-N48 possess triple bond with distance is 1.1556 Å, the C22-O26, O23-C24 and N33-N35 having double bond with distance is 1.2011 Å, 1.2178 Å and 1.2928 Å respectively. The maximum bond angle observed was between C3-C2-C8, measuring 131.2135º.

Molecular electrical potential surface: The calculation of charged regions within a molecule helps to determine the molecular interactions and the characteristics of chemical bonds. The charge distributions of molecules can be visualized in three dimensions through the molecular electrostatic potential surface. This is significant since it illustrates the molecule's size, shape and electrostatic potential (positive, negative and neutral) through colour gradients. The electrostatic potential increases in the order red < orange < yellow < green < blue. The colour code of the maps (Fig. 4) was found to be in the range of -5.278e-2 a.u (deepest red) to 5.278e-2 a.u. (deepest blue). The negative electrostatic potential is located on the

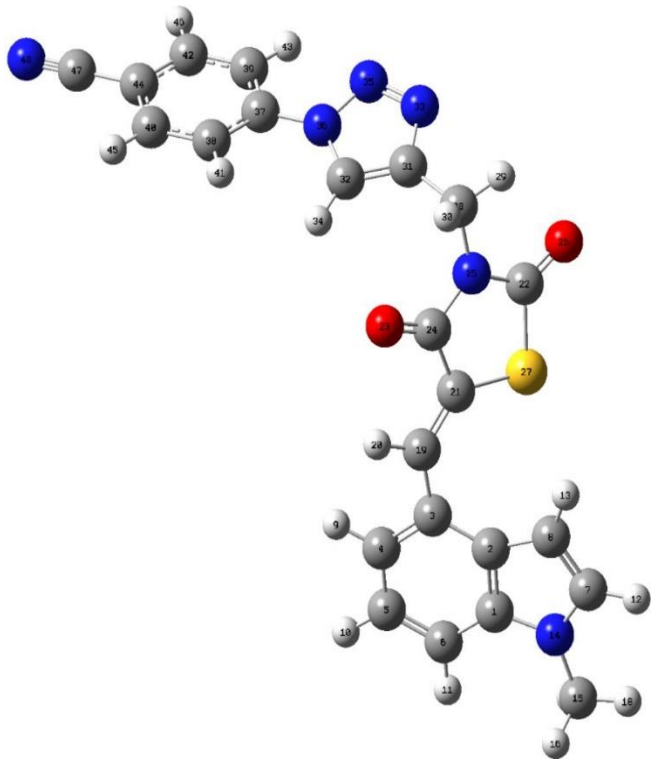

Fig. 3. Optimized geometrical structure of **7n** by using DFT calculations

TABLE-7
OPTIMIZED GEOMETRICAL PARAMETERS BOND LENGTH, BOND ANGLE AND DIHEDRAL ANGLES OF THE **7n** MOLECULE CALCULATED WITH B3LYP/6-311++G (d,p) BASIS SET

Bond lengths	Theoretical value (Å)	Bond lengths	Theoretical value (Å)	Bond lengths	Theoretical value (Å)
(C1–C2)	1.4267	(C15–H16)	1.0941	(C31–N33)	1.3680
(C1–C6)	1.3949	(C15–H17)	1.0931	(C32–H34)	1.0751
(C1–N14)	1.3799	(C15–H18)	1.0894	(C32–N36)	1.3611
(C2–C3)	1.4184	(C19–H20)	1.0880	(N33–N35)	1.2928
(C2–C8)	1.4324	(C19–C21)	1.3489	(N35–N36)	1.3637
(C3–C4)	1.4026	(C21–C24)	1.4867	(N36–C37)	1.4183
(C3–C19)	1.4581	(C21–S27)	1.7749	(C37–C38)	1.3969
(C4–C5)	1.3997	(C22–N25)	1.3921	(C37–C39)	1.3977
(C4–H9)	1.0845	(C22–O26)	1.2011	(C38–C40)	1.3878
(C5–C6)	1.3900	(C22–S27)	1.8046	(C38–H41)	1.0823
(C5–H10)	1.0835	(O23–C24)	1.2178	(C39–C42)	1.3865
(C6–H11)	1.0837	(C24–N25)	1.3922	(C39–H43)	1.0810
(C7–C8)	1.3705	(N25–C28)	1.4720	(C40–C44)	1.4014
(C7–H12)	1.0793	(C28–H29)	1.0890	(C40–H45)	1.0826
(C7–N14)	1.3782	(C28–H30)	1.0912	(C42–C44)	1.4029
(C8–H13)	1.0762	(C28–C31)	1.4981	(C42–H46)	1.0827
(N14–C15)	1.4512	(C31–C32)	1.3744	(C44–C47)	1.4302

Bond angles	Theoretical value (º)	Bond angles	Theoretical value (º)	Bond angles	Theoretical value (º)
A (2,1,6)	122.8380	A (14,15,17)	110.7595	A (28,31,33)	121.5359
A (2,1,14)	107.9487	A (14,15,18)	108.8962	A (32,31,33)	108.1797
A (6,1,14)	129.1621	A (16,15,17)	108.9506	A (31,32,34)	131.0745
A (1,2,3)	118.6734	A (16,15,18)	108.6235	A (31,32,36)	104.5475
A (1,2,8)	106.3635	A (17,15,18)	108.4435	A (34,32,36)	124.3309
A (3,2,8)	134.8531	A (3,19,20)	115.6434	A (31,33,35)	109.6527
A (2,3,4)	117.6177	A (3,19,21)	130.9081	A (33,35,36)	107.5295
A (2,3,19)	125.2054	A (20,19,21)	113.2991	A (32,36,35)	110.0898
A (4,3,19)	117.1762	A (19,21,24)	119.9396	A (32,36,37)	129.4613
A (3,4,5)	122.3235	A (19,21,27)	129.3955	A (35,36,37)	120.4489
A (3,4,9)	118.6434	A (24,21,27)	110.4094	A (36,37,38)	120.1959
A (5,4,9)	119.0067	A (25,22,26)	126.0947	A (36,37,39)	119.2765
A (4,5,6)	120.9405	A (25,22,27)	109.8451	A (38,37,39)	120.5273
A (4,5,10)	119.3792	A (26,22,27)	124.0554	A (37,38,40)	119.7586
A (6,5,10)	119.6798	A (21,24,23)	126.3439	A (37,38,41)	120.6146
A (1,6,5)	117.4985	A (21,24,25)	110.8763	A (40,38,41)	119.6199
A (1,6,11)	121.6109	A (23,24,25)	122.7787	A (37,39,42)	119.5771
A (5,6,11)	120.8769	A (22,25,24)	117.3113	A (37,39,43)	119.4410
A (8,7,12)	129.4902	A (22,25,28)	121.4569	A (42,39,43)	120.9818
A (8,7,14)	110.3626	A (24,25,28)	121.2030	A (38,40,44)	120.1857
A (12,7,14)	120.1471	A (21,27,22)	91.5531	A (38,40,45)	120.0135
A (2,8,7)	106.9891	A (25,28,29)	106.9043	A (44,40,45)	119.7976
A (2,8,13)	127.8619	A (25,28,30)	107.1850	A (39,42,44)	120.3764
A (7,8,13)	125.1461	A (25,28,31)	113.6956	A (39,42,46)	119.9398
A (1,14,7)	108.3117	A (29,28,30)	109.4442	A (44,42,46)	119.6822
A (1,14,15)	125.5680	A (29,28,31)	108.7161	A (40,44,42)	119.5698
A (7,14,15)	126.0483	A (30,28,31)	110.7683	A (40,44,47)	120.1423
A (14,15,16)	111.1028	A (28,31,32)	130.2827		
Dihedral angles	Theoretical value (º)	Dihedral angles	Theoretical value (º)	Dihedral angles	Theoretical value (º)
D (6,1,2,3)	-0.7182	D (8,7,14,15)	-177.7726	D (28,31,32,34)	-2.6985
D (6,1,2,8)	176.0256	D (12,7,14,1)	179.1695	D (28,31,32,36)	179.7735
D (14,1,2,3)	-178.3329	D (12,7,14,15)	2.1277	D (33,31,32,34)	177.7821
D (14,1,2,8)	-1.5891	D (1,14,15,16)	-62.9647	D (33,31,32,36)	0.2541
D (2,1,6,5)	-1.2710	D (1,14,15,17)	58.2705	D (28,31,33,35)	-179.6996
D (2,1,6,11)	-179.9376	D (1,14,15,18)	177.4377	D (32,31,33,35)	-0.1297
D (14,1,6,5)	175.8020	D (7,14,15,16)	113.5821	D (31,32,36,35)	-0.2919
D (14,1,6,11)	-2.8647	D (7,14,15,17)	-125.1827	D (31,32,36,37)	179.6893
D (2,1,14,7)	1.4425	D (7,14,15,18)	-6.0155	D (34,32,36,35)	-178.0354
D (2,1,14,15)	178.5021	D (3,19,21,24)	176.9504	D (34,32,36,37)	1.9459
D (6,1,14,7)	-175.9726	D (3,19,21,27)	3.3517	D (31,33,35,36)	-0.0538
D (6,1,14,15)	1.0870	D (20,19,21,24)	1.6656	D (33,35,36,32)	0.2222
D (1,2,3,4)	3.2014	D (20,19,21,27)	-171.933	D (33,35,36,37)	-179.7610
D (1,2,3,19)	-177.1004	D (19,21,24,23)	5.1325	D (32,36,37,38)	21.7088
D (8,2,3,4)	-172.3895	D (19,21,24,25)	-174.4812	D (32,36,37,39)	-158.5056
D (8,2,3,19)	7.3087	D (27,21,24,23)	179.8579	D (35,36,37,38)	-158.3116
D (1,2,8,7)	1.1401	D (27,21,24,25)	0.2441	D (35,36,37,39)	21.4740
D (1,2,8,13)	-178.2569	D (19,21,27,22)	174.228	D (36,37,38,40)	-179.4811
D (3,2,8,7)	177.1091	D (24,21,27,22)	0.1449	D (36,37,38,41)	1.4848
D (3,2,8,13)	-2.2879	D (26,22,25,24)	-178.4501	D (39,37,38,40)	0.7360
D (2,3,4,5)	-3.8752	D (26,22,25,28)	-0.3799	D (39,37,38,41)	-178.2981
D (2,3,4,9)	178.0148	D (27,22,25,24)	0.7755	D (36,37,39,42)	179.9970
D (19,3,4,5)	176.4021	D (27,22,25,28)	178.8457	D (36,37,39,43)	-0.1111
D (19,3,4,9)	-1.7080	D (25,22,27,21)	-0.4983	D (38,37,39,42)	-0.2181
D (2,3,19,20)	-146.3287	D (26,22,27,21)	178.7464	D (38,37,39,43)	179.6738
D (2,3,19,21)	38.4754	D (21,24,25,22)	-0.6728	D (37,38,40,44)	-0.6371
D (4,3,19,20)	33.3707	D (21,24,25,28)	-178.7482	D (37,38,40,45)	-179.9847
D (4,3,19,21)	-141.8252	D (23,24,25,22)	179.6972	D (41,38,40,44)	178.4068
D (3,4,5,6)	1.9324	D (23,24,25,28)	1.6219	D (41,38,40,45)	-0.9409
D (3,4,5,10)	-178.3181	D (22,25,28,29)	-13.2705	D (37,39,42,44)	-0.3966
D (9,4,5,6)	-179.9641	D (22,25,28,30)	-130.5395	D (37,39,42,46)	-179.9424
D (9,4,5,10)	-0.2146	D (22,25,28,31)	106.7047	D (43,39,42,44)	179.7132

D (4,5,6,1)	0.6978	D (24,25,28,29)	164.7247	D (43,39,42,46)	0.1674
D (4,5,6,11)	179.3748	D (24,25,28,30)	47.4558	D (38,40,44,42)	0.0295
D (10,5,6,1)	-179.0510	D (24,25,28,31)	-75.3001	D (38,40,44,47)	-179.8794
D (10,5,6,11)	-0.3740	D (25,28,31,32)	69.4054	D (45,40,44,42)	179.3785
D (12,7,8,2)	179.8317	D (25,28,31,33)	-111.1303	D (45,40,44,47)	-0.5304
D (12,7,8,13)	-0.7505	D (29,28,31,32)	-171.6499	D (39,42,44,40)	0.4919
D (14,7,8,2)	-0.2800	D (29,28,31,33)	7.8144	D (39,42,44,47)	-179.5993
D (14,7,8,13)	179.1378	D (30,28,31,32)	-51.3596	D (46,42,44,40)	-179.9611
D (8,7,14,1)	-0.7308	D (30,28,31,33)	128.1047	D (46,42,44,47)	-0.0524

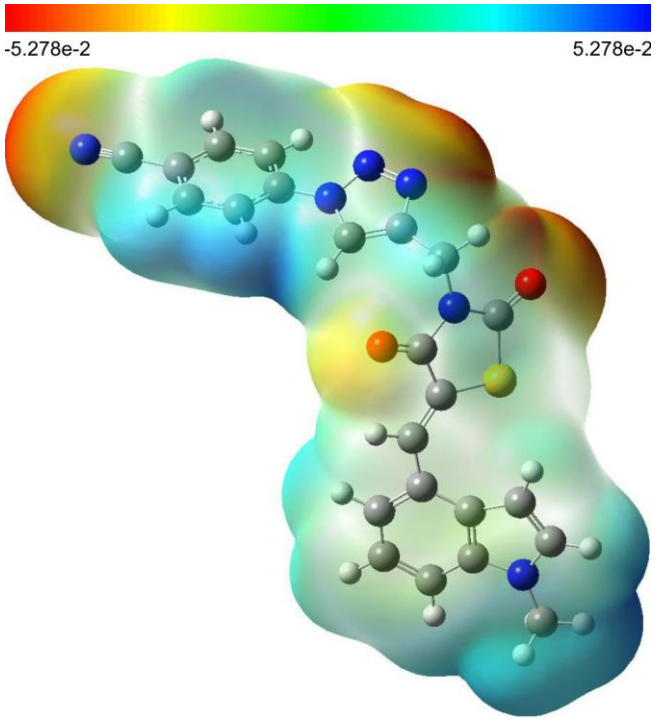

Fig. 4. Calculated MEP maps for **7n** molecule

oxygen atom of thiazolidine-dione and the nitrogen atoms of thiazolidine-2,4-dione, triazole and cyano-benzene. In contrast, the positive electrostatic potential is found on the hydrogen atoms attached to carbon atoms, represented by blue shades.

Electronic properties: The molecular orbital (MO) analysis of E_{HOMO} and E_{LUMO} is closely related to chemical reactivity and stability. These parameters provide insights into the molecule's ability to donate or accept electrons, which influences its reactivity and overall stability. Compound **7n** exhibits a HOMO–LUMO energy gap (ΔE) of 3.54370 eV (Fig. 5 and Table-8).

Mulliken atomic charges: Mulliken atomic charges of compound **7n** have been computed using the DFT/B3LYP/6-311G++ (d,p) basis set and are collected in Table-9, where it could be seen that the six carbon C2, C3, C21, C32, C38 and C44 atoms of **7n** molecule possess positive charges and seventeen C1, C4, C5, C6, C7, C8, C15, C19, C22, C24, C28, C31, C37, C39, C40, C42 and C47 atoms possess negative charges (Fig. 6). Similar to the Mulliken atomic charges, here, the N14, N25, S27, N33 and N36 possess positive charges and O23, O26, N35 and N48 atoms possess high electronegativity. Besides, the positive charge distribution observed on the all hydrogen atoms.

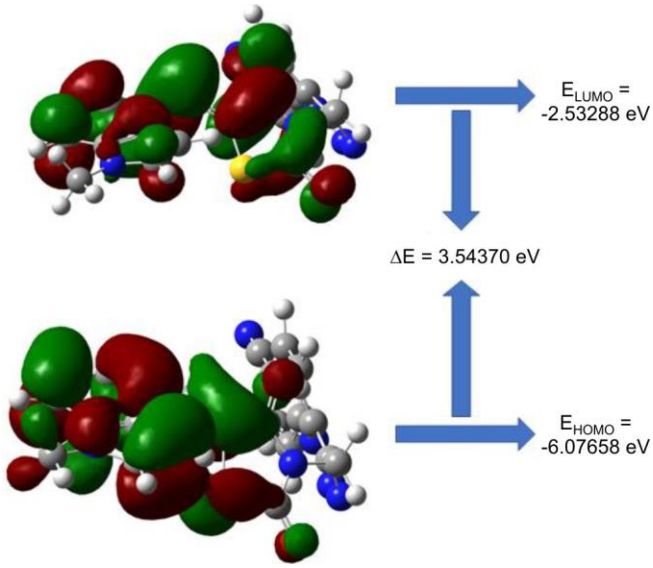

Fig. 5. Frontier molecular orbital energy gap of **7n** molecule

TABLE-8
THE CALCULATED FRONTIER MOLECULAR ORBITAL (FMO)s RELATED TO THE GLOBAL REACTIVITY DESCRIPTORS OF **7n** MOLECULE

Property	B3LYP/6-311G++ (d,p)
E_{HOMO} (eV)	-6.07658
E_{LUMO} (eV)	-2.53288
Energy gap (eV)	3.54370
Ionization potential (I) (eV)	6.07658
Electron affinity (A) (eV)	2.53288
Electronegativity (χ) (eV)	4.30473
Global hardness (η) (eV)	1.77185
Chemical potential (μ) (eV)	-4.30473
Global electrophilicity (ω) (eV)	5.22928
Chemical softness (S) (eV)	0.88593

eV: electron volt, ($I = -E_{HOMO}$), electron affinity ($A = -E_{LUMO}$), electronegativity [$\chi = (I+A/2)$], global hardness [$\eta = (I-A/2)$], chemical softness ($S = 1/2\eta$), electronic chemical potential [$\mu = -(I+A/2)$] and electrophilicity ($\omega = \mu^2/2\eta$). All these parameters are listed in Table-8.

Conclusion

Few new hybrid molecules (**7a-o**) consisting of indole, thiazolidinedione and 1,2,3-triazole as pharmacophores were synthesized and screened for *in vitro* anticancer activity by taking three human cancer cell lines such as A549, MCF-7 and HeLa. Out of all, compounds **7a**, **7c**, **7g**, **7l** and **7n** displayed predominant activity than the nocodazole towards tested cell lines with IC_{50} values < 1.5 μM. Similarly, *in vitro* tubulin

TABLE-9
CALCULATED MULLIKEN ATOMIC CHARGES OF **7n** MOLECULE

S. No	Atoms	Mulliken atomic charges	S. No	Atoms	Mulliken atomic charges
1	C	-0.011288	25	N	0.550402
2	C	0.007257	26	O	-0.265563
3	C	0.464562	27	S	0.066592
4	C	-0.157027	28	C	-0.983309
5	C	-0.463769	29	H	0.247165
6	C	-0.035682	30	H	0.227904
7	C	-0.132553	31	C	-0.433545
8	C	-0.358122	32	C	0.461986
9	H	0.142138	33	N	0.082575
10	H	0.177465	34	H	0.235295
11	H	0.158735	35	N	-0.039714
12	H	0.179499	36	N	0.324476
13	H	0.147474	37	C	-0.300972
14	N	0.115631	38	C	0.142036
15	C	-0.284323	39	C	-0.178601
16	H	0.180878	40	C	-0.127807
17	H	0.175029	41	H	0.140892
18	H	0.145999	42	C	-0.445222
19	C	-0.441154	43	H	0.240799
20	H	0.259046	44	C	1.949530
21	C	0.910365	45	H	0.220054
22	C	-0.120947	46	H	0.209564
23	O	-0.267348	47	C	-1.738637
24	C	-1.225400	48	N	-0.152366

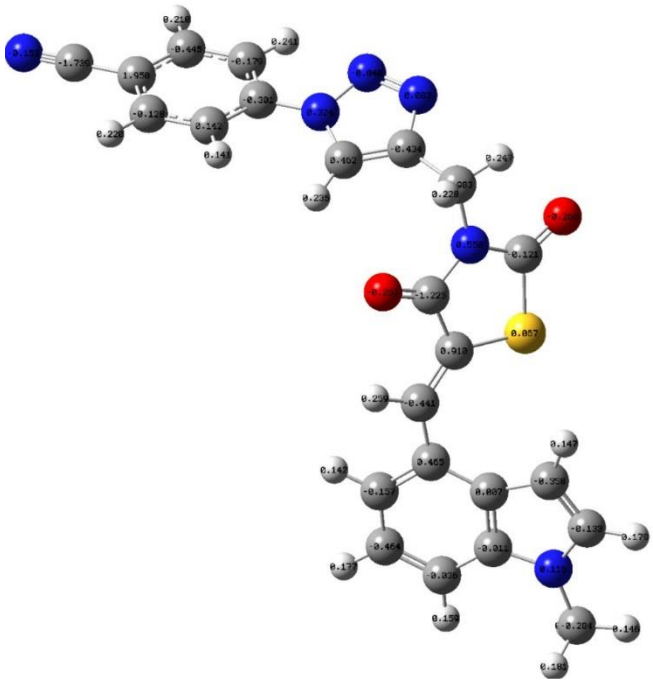

Fig. 6. Mulliken atomic charges of **7n** molecule

polymerization inhibition assay revealed that compounds **7c**, **7g**, **7l** and **7n** showed more inhibition than the standard CA-4. Molecular docking studies revealed the important binding interactions of compounds **7a**, **7c** and **7n** on α,β-tubulin (PDB ID 4HJO) and same compounds showed better binding energies and inhibition constants than the nocodazole. Further the results of *in silico* pharmacokinetic profile (ADMET) revealed that compounds **7a**, **7c** and **7n** followed all the rules of Lipinski, Veber, Egan and Muegge without any deviation. Finally, DFT with the B3LYP/6–311++G(d,p) basis set was used to the characterize compound **7n**.

CONFLICT OF INTEREST

The authors declare that there is no conflict of interests regarding the publication of this article.

REFERENCES

1. A. Kumari and R.K. Singh, *Bioorg. Chem.*, **89**, 103021 (2019); https://doi.org/10.1016/j.bioorg.2019.103021
2. S. Kumar and Ritika, *Futur. J. Pharm. Sci.*, **6**, 121 (2020); https://doi.org/10.1186/s43094-020-00141-y
3. M.Z. Zhang, Q. Chen and G.F. Yang, *Eur. J. Med. Chem.*, **89**, 421 (2015); https://doi.org/10.1016/j.ejmech.2014.10.065
4. T.V. Sravanthi and S.L. Manju, *Eur. J. Pharm. Sci.*, **91**, 1 (2016); https://doi.org/10.1016/j.ejps.2016.05.025
5. S. Dadashpour and S. Emami, *Eur. J. Med. Chem.*, **150**, 9 (2018); https://doi.org/10.1016/j.ejmech.2018.02.065
6. M.E. Welsch, S.A. Snyder and B.R. Stockwell, *Curr. Opin. Chem. Biol.*, **14**, 347 (2010); https://doi.org/10.1016/j.cbpa.2010.02.018
7. F.R. deSaAlves, E.J. Barreiro and C.A.M. Fraga, *Mini Rev. Med. Chem.*, **9**, 782 (2009); https://doi.org/10.2174/138955709788452649
8. B.E. Evans, K.E. Rittle, M.G. Bock, R.M. DiPardo, R.M. Freidinger, W.L. Whitter, G.F. Lundell, D.F. Veber, P.S. Anderson, R.S.L. Chang, V.J. Lotti, D.J. Cerino, T.B. Chen, P.J. Kling, K.A. Kunkel, J.P. Springer and J. Hirshfield, *J. Med. Chem.*, **31**, 2235 (1988); https://doi.org/10.1021/jm00120a002
9. S. Verma and Y. Prabhakar, *Curr. Med. Chem.*, **22**, 1603 (2015); https://doi.org/10.2174/0929867322666150209151209
10. D. Sunil and P.R. Kamath, *Curr. Top. Med. Chem.*, **17**, 959 (2017); https://doi.org/10.2174/1568026616666160927150839
11. F. Naaz, K. Neha, M.R. Haider and S. Shafi, *Future Med. Chem.*, **13**, 1795 (2021); https://doi.org/10.4155/fmc-2020-0385
12. M.E. Welsch, S.A. Snyder and B.R. Stockwell, *Curr. Opin. Chem. Biol.*, **14**, 347 (2010); https://doi.org/10.1016/j.cbpa.2010.02.018
13. Q. Zhang, H. Zhou, S. Zhai and B. Yan, *Curr. Pharm. Des.*, **16**, 1826 (2010); https://doi.org/10.2174/138161210791208983
14. O. Bozdağ-Dündar, Ö. Özgen, A. Menteşe, N. Altanlar, O. Atlı, E. Kendi and R. Ertan, *Bioorg. Med. Chem.*, **15**, 6012 (2007); https://doi.org/10.1016/j.bmc.2007.06.049
15. C.D. Barros, A.A. Amato, T.B. Oliveira, K.B.R. Iannini, A.L. Silva, T.G. Silva, E.S. Leite, M.Z. Hernandes, M.C.A. Lima, S.L. Galdino, F.A.R. Neves and I.R. Pitta, *Bioorg. Med. Chem.*, **18**, 3805 (2010); https://doi.org/10.1016/j.bmc.2010.04.045
16. N. Swathi, Y. Ramu, C.V.S. Subrahmanyam and K. Satyanarayana, *Int. J. Pharma Sci.*, **4**, 561 (2012).
17. S.R. Pattan, K.R. Alagwadi, A.R. Bhat, V.V.K. Reddy, J.S. Pattan and A.B. Khade, *Indian Drugs*, **45**, 532 (2008).
18. Y. Momose, T. Maekawa, T. Yamano, M. Kawada, H. Odaka, H. Ikeda and T. Sohda, *J. Med. Chem.*, **45**, 1518 (2002); https://doi.org/10.1021/jm010490l
19. S.A. El-Feky, *Pharmazie*, **48**, 894 (1993).
20. M.P. Ip, P.W. Sylvester and L. Schenkel, *Cancer Res.*, **46**, 1735 (1986).
21. V. Asati, D.K. Mahapatra and S.K. Bharti, *Eur. J. Med. Chem.*, **87**, 814 (2014); https://doi.org/10.1016/j.ejmech.2014.10.025
22. W. Li, Y. Lu, Z. Wang, J.T. Dalton and D.D. Miller, *Bioorg. Med. Chem. Lett.*, **17**, 4113 (2007); https://doi.org/10.1016/j.bmcl.2007.05.059

23. C.S. Ananda Kumar, C.V. Kavitha, K. Vinaya, S.B. Prasad, N.R. Thimmegowda, S. Chandrappa, S.C. Raghavan and K.S. Rangappa, *Invest New Drugs*, **27**, 327 (2009); https://doi.org/10.1007/s10637-008-9179-3
24. Z. Beharry, M. Zemskova, S. Mahajan, F. Zhang, J. Ma, Z. Xia, M. Lilly, C.D. Smith and A.S. Kraft, *Mol. Cancer Ther.*, **8**, 1473 (2009); https://doi.org/10.1158/1535-7163.MCT-08-1037
25. J. Xie, Q. Li, X. Ding and Y. Gao, *Oncotarget*, **8**, 50814 (2017); https://doi.org/10.18632/oncotarget.15135
26. K. Liu, W. Rao, H. Parikh, Q. Li, T.L. Guo, S. Grant, G.E. Kellogg and S. Zhang, *Eur. J. Med. Chem.*, **47**, 125 (2012); https://doi.org/10.1016/j.ejmech.2011.10.031
27. E.K. Keeton, K. McEachern, K.S. Dillman, S. Palakurthi, Y. Cao, M.R. Grondine, S. Kaur, S. Wang, Y. Chen, A. Wu, M. Shen, F.D. Gibbons, M.L. Lamb, X. Zheng, R.M. Stone, D.J. DeAngelo, L.C. Platanias, L.A. Dakin, H. Chen, P.D. Lyne and D. Huszar, *Blood*, **123**, 905 (2014); https://doi.org/10.1182/blood-2013-04-495366
28. Y.W. Lin, Z.M. Beharry, E.G. Hill, J.H. Song, W. Wang, Z. Xia, Z. Zhang, P.D. Aplan, J.C. Aster, C.D. Smith and A.S. Kraft, *Blood*, **115**, 824 (2010); https://doi.org/10.1182/blood-2009-07-233445
29. K. Lal and P. Yadav, *Anticancer. Agents Med. Chem.*, **18**, 21 (2018); https://doi.org/10.2174/1871520616666160811113531
30. J. Akhtar, A.A. Khan, Z. Ali, R. Haider and M.S. Yar, *Eur. J. Med. Chem.*, **125**, 143 (2017); https://doi.org/10.1016/j.ejmech.2016.09.023
31. M.M. Alam, *Arch. Pharm. (Weinheim)*, **355**, 2100158 (2022); https://doi.org/10.1002/ardp.202100158
32. D. Lengerli, K. Ibis, Y. Nural and E. Banoglu, *Expert Opin. Drug Discov.*, **17**, 1209 (2022); https://doi.org/10.1080/17460441.2022.2129613
33. A. Vanaparthy, K. Bokkala, N.S. Thirukovela, N. Sirassu, R. Manchal, B. Srinivas and S.K. Nukala, *ChemistrySelect*, **8**, e202301179 (2023); https://doi.org/10.1002/slct.202301179
34. S. Senapati, A.K. Mahanta, S. Kumar and P. Maiti, *Signal Transduct. Target. Ther.*, **3**, 7 (2018); https://doi.org/10.1038/s41392-017-0004-3
35. N. Kumar and N. Goel, *Anticancer. Agents Med. Chem.*, **22**, 3196 (2022); https://doi.org/10.2174/1871520622666220404082648
36. P. Martins, J. Jesus, S. Santos, L. Raposo, C. Roma-Rodrigues, P. Baptista and A. Fernandes, *Molecules*, **20**, 16852 (2015); https://doi.org/10.3390/molecules200916852
37. B. Shankar, P. Jalapathi, B. Saikrishna, S. Perugu and V. Manga, *Chem. Cent. J.*, **12**, 1 (2018); https://doi.org/10.1186/s13065-017-0364-3
38. F. Naaz, M.R. Haider, S. Shafi and M.S. Yar, *Eur. J. Med. Chem.*, **171**, 310 (2019); https://doi.org/10.1016/j.ejmech.2019.03.025
39. R. Kaur, G. Kaur, R.K. Gill, R. Soni and J. Bariwal, *Eur. J. Med. Chem.*, **87**, 89 (2014); https://doi.org/10.1016/j.ejmech.2014.09.051
40. S. Boda, S.K. Nukala and R. Manchal, *ChemistrySelect*, **7**, e202200972 (2022); https://doi.org/10.1002/slct.202200972
41. M.S. Reddy, N.S. Thirukovela, S. Narsimha, M. Ravinder, S. K. Nukala, *J. Mol. Struct.*, **1250**, 131747 (2022); https://doi.org/10.1016/j.molstruc.2021.131747
42. M.S. Reddy, T.N. Swamy, M. Ravinder and S.K. Nukala, *Russ. J. Gen. Chem.*, **91**, 1135 (2021); https://doi.org/10.1134/S1070363221060232
43. B. Karthik, T.N. Swamy, A.K. Kumar, M. Ravinder and S.K. Nukala, *Russ. J. Bioorg. Chem.*, **47**, 1269 (2021); https://doi.org/10.1134/S1068162021060091
44. S.R. Bandi, N. Kavitha, S.K. Nukala, N.S. Thirukovela, R. Manchal, R. Palabindela and S. Narsimha, *J. Mol. Struct.*, **1274**, 134378 (2023); https://doi.org/10.1016/j.molstruc.2022.134378
45. M. Kumar, S.K. Nukala, T.M. Krishna and S. Narsimha, *J. Mol. Struct.*, **1250**, 131722 (2022); https://doi.org/10.1016/j.molstruc.2021.131722
46. Y. Bonakolluru, S.K. Nukala, G. Dasari, V. Badithapuram, R. Manchal and S. Bandari, *Polycycl. Aromat. Compd.*, **43**, 6319 (2023); https://doi.org/10.1080/10406638.2022.2117208
47. C.V. Junior, A. Danuello, V.S. Bolzani, E.J. Barreiro and C.A.M. Fraga, *Curr. Med. Chem.*, **14**, 1829 (2007); https://doi.org/10.2174/092986707781058805
48. L.K. Gediya and V.C. Njar, *Expert Opin. Drug Discov.*, **4**, 1099 (2009); https://doi.org/10.1517/17460440903341705
49. E. Hamel, *Cell Biochem. Biophys.*, **38**, 1 (2003); https://doi.org/10.1385/CBB:38:1:1
50. R. Ravelli, B. Gigant, P. Curmi, I. Jourdain, S. Lachkar, A. Sobel and M. Knossow, *Nature*, **428**, 198 (2004); https://doi.org/10.1038/nature02393
51. D.R.V. Pires, T.L. Blundell and D.B. Ascher, *J. Med. Chem.*, **58**, 4066 (2015); https://doi.org/10.1021/acs.jmedchem.5b00104
52. A. Daina, O. Michielin and V. Zoete, *Sci. Rep.*, **7**, 42717 (2017); https://doi.org/10.1038/srep42717